Agricultural Water Management 284 (2023) 108359

Contents lists available at ScienceDirect

Agricultural Water Management

journal homepage: www.elsevier.com/locate/agwat

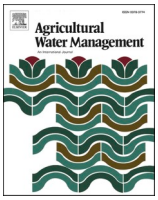

Probabilistic assessment of drought impacts on wheat yield in south-eastern Australia

Keyu Xiang [a,b], Bin Wang [b,*], De Li Liu [b,c,**], Chao Chen [d], Cathy Waters [e], Alfredo Huete [a], Qiang Yu [f]

[a] School of Life Sciences, Faculty of Science, University of Technology Sydney, PO Box 123, Broadway, Sydney, NSW 2007, Australia
[b] NSW Department of Primary Industries, Wagga Wagga Agricultural Institute, Wagga Wagga, NSW 2650, Australia
[c] Climate Change Research Centre, University of New South Wales, Sydney, NSW 2052, Australia
[d] CSIRO Agriculture and Food, Private Bag 5, PO Wembley, WA 6913, Australia
[e] NSW Department of Primary Industries, Dubbo NSW 2830, Australia
[f] State Key Laboratory of Soil Erosion and Dryland Farming on the Loess Plateau, Northwest A&F University, Yangling, Shaanxi 712100, China

ARTICLE INFO

Handling Editor - Dr. B.E. Clothier

Keywords:
Wheat yield
Drought index
Copula-based function
Yield loss probability
Drought threshold

ABSTRACT

A risk-based approach is more meaningful to quantify the effects of drought on crop yield given the randomness nature of past drought events, compared to the deterministic approach. However, the majority of these probabilistic studies are conducted at national or global scale to assess the yield loss probability under given drought conditions. There is still a lack of research combining droughts and crop yields in a probabilistic way at a local scale. Moreover, it is unclear how drought threshold triggering yield loss at a given conditional probability will vary in dryland cropping regions. Here, we used wheat yield data from 66 shires in New South Wales (NSW) wheat belt and meteorological data from 986 weather stations. A copula-based probabilistic method was developed to explore the yield loss probability to various drought conditions. We investigated the drought threshold under a given yield loss probability using the constructed copula function. We found that SPEI-6 in October was the optimal drought index to represent detrended wheat yield variation as this period covered the main growth stages of winter wheat in the study region. Our results show that as the severity of drought increased, the wheat yield loss probability also increased. Yield loss probability varied among the study shires, mainly due to the various climate conditions of each region. The drought threshold in subregion 1 (the northwest) was highest, followed by subregion 2 (the southwest) and subregion 3 (the eastern), indicating that wheat yield in subregion 1 was more sensitive to drought. The findings could provide important direction and benchmarks for stakeholders in evaluating the agricultural impact of drought, especially in those drought prone areas. We expect that the methodological framework developed here can be extended to other dryland areas to provide helpful information to growers, risk management policy makers and agricultural insurance evaluators.

1. Introduction

Climate variability can cause various natural hazards (Loukas et al., 2008; Sun et al., 2023; Yin et al., 2022), with drought being one of the most common hazards around the world (Chiang et al., 2021; Christian et al., 2021; Meza et al., 2021). Drought can lead to several negative effects on ecosystem, including but not limited to, carbon and water cycle (Hoover et al., 2022; Yang et al., 2016), vegetation growth (Ding et al., 2020b; He et al., 2022), and water resources (Chang et al., 2019; Li et al., 2022b). One of the most relevant to human society is the negative impact on crop production, which has become a very serious issue, especially in those regions and countries where crop is vulnerable to drought (Araneda-Cabrera et al., 2021; Deb et al., 2022; Li et al., 2021). For example, global yields of wheat and maize can be reduced by 40 % and 21 %, respectively, when the water availability ratio was reduced to 50 % caused by drought events (Daryanto et al., 2016).

Different drought conditions cause varied magnitudes of yield loss. To quantify the effects of the various drought conditions, drought index, such as Standardized Precipitation Index (SPI) (McKee et al., 1993) and Standardized Precipitation Evapotranspiration Index (SPEI), has been

* Corresponding author.
** Corresponding author at: NSW Department of Primary Industries, Wagga Wagga Agricultural Institute, Wagga Wagga, NSW 2650, Australia.
E-mail addresses: bin.a.wang@dpi.nsw.gov.au (B. Wang), de.li.liu@dpi.nsw.gov.au (D.L. Liu).

https://doi.org/10.1016/j.agwat.2023.108359
Received 21 March 2023; Received in revised form 8 May 2023; Accepted 9 May 2023
Available online 16 May 2023

developed and implemented to quantify drought characteristics. SPI is the most commonly used meteorological drought index as it is easy to compute with only precipitation data. It was used as the standard to compare with other indices (Soľáková et al., 2014; Szalai and Szinell, 2000). Additionally, SPEI, proposed by Vicente-Serrano et al. (2010), was widely used because it adopts a similar mechanism theory to the SPI and takes potential evapotranspiration (PET) into account to provide a more realistic description of the water variability in the study area. Wang et al. (2015b) assessed the change of long-term (1961–2012) drought severity in China with SPI and SPEI. They found that SPI/SPEI was able to characterize the evolution of the wet and dry conditions of the study region. Haile et al. (2020) analysed drought pattern on monthly, seasonal and interannual basis with SPEI at various timescales in the Greater Horn of Africa. The results showed that drought was more frequent and persistent in Sudan and Tanzania, but more severe in Somalia, Ethiopia and Kenya.

The characteristics of the effects of droughts on crop yield can be captured by the drought index (Araneda-Cabrera et al., 2021; Mokhtar et al., 2022). But the suitability of SPI and SPEI was highly dependent on the study area and crop types. For example, Chen et al. (2020b) compared the relationship between multiple drought indices and crop yield at different time scales. They found that the reliability of yield variation analysis was influenced by the choice of drought indices and time scales. Labudová et al. (2017) investigated the correlation between dry/wet conditions and crop yields in Danubian Lowland and the East Slovakian Lowland with SPI and SPEI. They found that the SPEI had a higher correlation with yield fluctuations for most crops than SPI except potato. Thus, it is important to identify the optimal drought index at different time scales to evaluate the effects of drought on crop yield in a given study area (Kamali et al., 2022; Prodhan et al., 2022).

Both statistical models and process-based crop models have been widely used to evaluate the effects of drought events on crop yield. For example, Zhang et al. (2019) used CERES-Maize model based on risk assessment theory to construct a dynamical drought risk assessment model for maize and analysed the drought impacts on maize yield in north-eastern China. They found that the hazard level caused by drought varied in the different growth stages of maize. In Iran, Zarei et al. (2019) tested the R^2 coefficients between several climate indices and wheat yield loss simulated by AquaCrop model. They found that selecting optimal index to assess climate change impacts on crop yield was required in different regions. As we all know, process-based crop models use the parameters calibrated in a few locations to simulate crop yield at a large area. However, this approach introduces uncertainties when they are applied beyond locations/regions where they are originally developed (Leng, 2021). Moreover, statistical models are used to study the impacts of droughts on crop yields by fitting a linear or non-linear relationships between long-term historical yield and observed climate variables (Kamali et al., 2015; Wambua, 2019). The advantage of such empirical analysis is to provide the overall sensitivity of yield response to drought given its simplicity and less computation cost. Recently, a risk-based approach is more meaningful to study the effects of drought on crop yield given the randomness nature of drought events (Feng and Hao, 2020; Ribeiro et al., 2019a). As one of probability-based statistical approaches, copula function is getting more widely used because of its capability of linking several variables to obtain their joint probabilities (Sklar, 1973). Copula can establish the joint distribution function of variables via combining the marginal distribution functions of different variables (Patton, 2012; Poonia et al., 2021). Integrated with the conditional probability theory, copula enables estimating the probability of crop yield loss under various drought scenarios. It can provide more valuable information to the practitioners when designing agricultural risk policies compared to the deterministic approach (Liu et al., 2022; Ribeiro et al., 2019a).

Australia is a significant player in the global grain trade and has been a major exporter of wheat for several years (Grundy et al., 2016; Zeleke and Nendel, 2016). The New South Wales (NSW) wheat belt is the main wheat production area of Australia, accounting for 27 % of the national production (www.abares.gov.au, 2013–14). However, the wheat in this region is grown under rainfed conditions and its yield is highly variable due to great climate variability. Almost half of the total production variation was caused by inter-annual variability of precipitation and temperature in south-eastern Australia (Ray et al., 2015; Waha et al., 2022). The recent 2018 drought in NSW resulted in local crop yields being about 53 % lower than the 20-year average (1999–2018) (Steve et al., 2018). Numerous studies investigated the impacts of historical climate variations on agricultural production in Australia (Feng et al., 2018; Potgieter et al., 2013; Wang et al., 2015a), but the majority of their conclusions are based on deterministic approaches, which are unable to provide any risk assessment information. Nevertheless, Madadgar et al. (2017) used copula functions to investigate drought impacts on five main crops at a national scale in Australia. The use of copula-based probabilistic approach to assess the probability of yield loss under given drought conditions has not been investigated at a local scale in Australia (Godfrey et al., 2022). Furthermore, it is not clear how drought threshold triggering yield loss at a given conditional probability will vary with different regions in Australian dryland cropping areas (Liu et al., 2022).

Here, we used a copula-based probabilistic method to explore the potential response of yield loss to various drought conditions in NSW wheat belt of south-eastern Australia based on long-term historical observed wheat yield and climate data for 66 shires. We aim to (1) identify the optimum drought index within the wheat growing season determining yield variation in the NSW wheat belt, (2) select marginal distribution function and establish the copula-based joint distribution function to quantify the probability of yield loss under different drought conditions for each shire, and (3) identify drought threshold triggering yield loss at a given conditional probability in the study region.

2. Materials and methods

2.1. Study area and data sources

The NSW wheat-belt (141.0°−152.0°E, 28.5°−36.1°S) is located in the south-eastern Australia and covers an area of 360,000 km^2 (Liu et al., 2014). The large parts of the NSW wheat belt are characterized by Mediterranean climate with a large interannual variation of precipitation. The western part of the NSW belt is warm and dry, while in contrast, the eastern part is cold and wet (Feng et al., 2018). The annual mean amount of precipitation varies from 200 mm in southwest to 1000 mm in southeast, while the annual mean temperature decreases from 20 °C in the northwest part to 11 °C towards the southeast part (Feng et al., 2019a).

There are 66 shires in the NSW wheat-belt, where the harvest area of wheat was nearly double up from 2123 to 3800 kha and the production increased almost four times from 3432 kt to 13,110 kt during the last several decades (ABARES: https://www.agriculture.gov.au). In our study, the wheat-growing region was separated into three sub-areas based on climatic conditions (Fig. 1) (Wang et al., 2015a). We selected six shires to represent the specific climatic characteristics of each region, and then these shires were used to demonstrate the probabilistic analysis at a shire-scale. Coonabarabbran (CB) and Moree Plains (MP) are relatively warm, Wakool (WK) and Narromine (NM) are relatively dry, Nundle (ND) and Gundagai (GD) are relatively cool and wet sites.

We used the historical climate data, including daily precipitation (P), maximum and minimum temperature (T_{max} and T_{min}), which were extracted from SILO patched point dataset (Jeffrey et al., 2001). We obtained the annual wheat yield data of 66 shires from Fitzsimmons (2001). The principal characteristics of all shires in the entire study region are summarized in Supplementary Table S1.

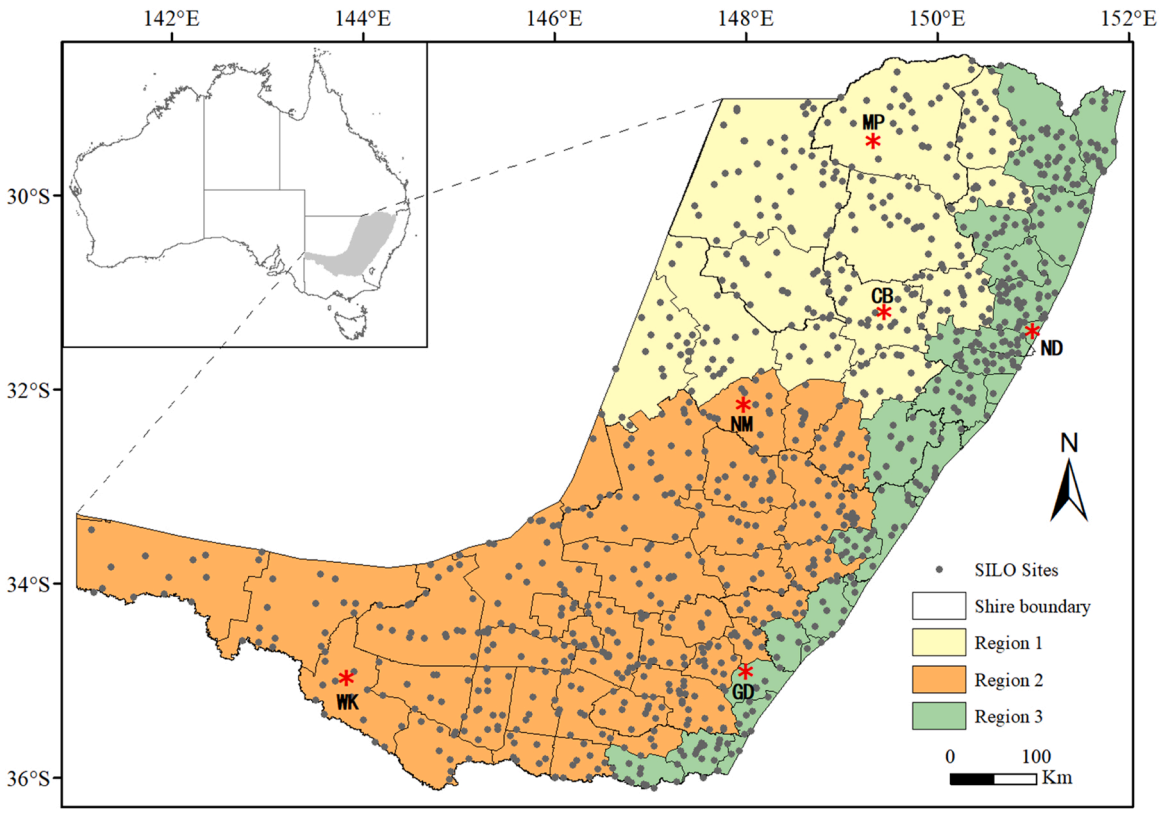

Fig. 1. Locations of the 66 shires and 986 SILO climate sites (grey dots) in the NSW wheat belt of south-eastern Australia. Six selected shires (red stars) including Coonabarabbran (CB), Moree Plains (MP), Wakool (WK), Narromine (NM), Nundle (ND), and Gundagai (GD) were used to demonstrate the probabilistic analysis.

2.2. Yield detrend

The NSW wheat yield has experienced a significant increase in recent decades as a result of improvements in agricultural management and technology (Wang et al., 2015a). The non-climatic factor should be removed before quantifying the drought impact on the wheat yield. First difference (*FD*) has been widely used to remove the influence of non-climatic factors (Tao et al., 2008; Zhang et al., 2010) by calculating the difference of crop yield between two successive year (Wang et al., 2015a),

$$\Delta Yield = Yield_i - Yield_{i\text{-}1} \quad (1)$$

where $\Delta Yield$ is the first difference of wheat yield (i.e., detrended yield), $Yield_i$ is the original yield for the ith year, $Yield_{i\text{-}1}$ is the original yield for the (i-1)th year, i starts from 1923 or 1961 in this study.

To ensure a comprehensive analysis and minimize biases caused by relying on a single detrend method, three additional detrended methods including Centre Moving Average (CMA) (Li et al., 2022c; Lu et al., 2017), Hodrick-Prescott (HP) filter (Cheng and Yin, 2021; Harvey and Trimbur, 2008), and Holt Exponential Smoothing (HES) (Holt, 2004; Li, 2013) were taken into consideration in our study. These alternative methods were employed to compare the detrended yield and provide a more robust understanding of the yield data. The specific equations and compared results of these three methods are listed in the supplementary materials.

2.3. Drought index

We used SPI and SPEI to investigate the impact of drought conditions on wheat yield variation. The SPI transforms the fitted distribution of precipitation record into a normal distribution with equiprobability transformation, and then zero is set as the mean value. Therefore, the values above or below zero represent the wet and dry conditions, respectively (McKee et al., 1993; Zargar et al., 2011). Also, we adopted this process into the construction of SPEI. However, we used the water balance (instead of precipitation), because it is the difference between precipitation and potential evapotranspiration (PET), to fit distribution (Vicente-Serrano et al., 2010). We selected the Thornthwaite model (Thornthwaite, 1948) to obtain the PET since the calculation procedure was simple and only mean temperature data was needed. As wheat growing season was April to November, the 3-month (Jul.-Sep., Aug.-Oct., and Sep.-Nov.) and 6-month (Apr.-Sep., May-Oct., and Jun.-Nov.) scales were used to calculate SPI and SPEI. For example, SPI-3-Sep. is the 3-month scale (Jul.-Sep.) in September, SPI-6-Sep. is the 6-month scale (Apr.-Sep.) in September. The classification of the two drought indices is shown in the Table 1 (McKee et al., 1993).

2.4. Optimal index selection

We used the Kendall tau correlation coefficient to select the drought index (Bonett and Wright, 2000; Croux and Dehon, 2010). We selected the index that had the highest tau value with detrended yield as the optimal drought index (DI_o) to reflect the impacts of drought on yield variation, and then we used this index to estimate the yield loss probabilities with the conditional values that represent the different drought severities. The tau coefficients calculated by the following equation (Temizhan et al., 2022):

Table 1
Classification standard for SPI and SPEI.

Drought severity	SPI/SPEI
Mild drought	(−1, −0.5]
Moderate drought	(−1.5, −1]
Severe drought	(−2, −1.5]
Extreme drought	(-∞, −2]

$$\tau = \frac{n_{\text{concordant}} - n_{\text{discordant}}}{n(n-1)/2} \quad (2)$$

where $n_{\text{concordant}}$ is the number of concordant pairs of drought index and detrended yield, $n_{\text{discordant}}$ is the number of discordant pairs, n is the number of pairs.

2.5. Probabilistic estimation of drought impacts on yield loss

2.5.1. Copula

Copula function initially proposed by Sklar (1973) is able to obtain the joint distribution by connecting the marginal distribution of any two or more variables depending on their correlation levels. It was previously used to estimate financial risk issues. Copula function is becoming more popular in the climatic hazards risk modelling due to less limitation on dependence of marginal functions and simplicity in construction (Won et al., 2020; Zhang and Jiang, 2019). A detailed description of copula can be obtained in Nelsen (2007). Here, we used a 2-dimensional copula function to model the joint distribution of drought index (x) and detrended yield (y), as shown in Eq. (3):

$$F_{x,y}(x,y) = C[F_x(x), F_y(y)] \quad (3)$$

where F is the marginal distributions of related variables, C is the cumulative distribution function of copula.

There are numerous copula functions that enable the description of the joint probability, dependence, and relationships between univariate variables under extreme situations (Nelsen, 2007). We compared six commonly used copula functions including Gaussian, t, Clayton, Gumbel, Frank, and Joe (Table 2) and fitted these functions in each shire. We used the Akaike information criterion (AIC) as the selection standard in the marginal distribution and copula fitting (Sakamoto et al., 1986). The smaller the AIC value showed the better fitting result.

Prior to the construction of copula function, the distribution of variables needs to be fitted. We used Normal distribution to fit drought index because SPI and SPEI conformed to the normal distribution according to their principle. Additionally, the Normal, Logistic, and Uniform distributions (Table 3) were used to fit the detrended yield for each shire.

2.5.2. Estimating conditional yield loss probability under different drought conditions

Based on the copula joint distribution, the conditional probability of yield loss under drought and non-drought conditions were estimated by Eqs. (4) and (5), respectively (Ribeiro et al., 2019b). We used different levels of drought severity, i.e., $X = -0.5, -0.75, -1, -1.25, -1.5$, and -1.75 as the different conditional values of DI_o. We set the conditional value of $\Delta Yield$ to -0.5, i.e., $Y = -0.5$, which represented the average yield loss.

$$\mathrm{P}(\mathrm{y} \le \mathrm{Y} \mid \mathrm{x} \le \mathrm{X}) = \frac{\mathrm{P}(\mathrm{x} \le \mathrm{X},\ \mathrm{y} \le \mathrm{Y})}{\mathrm{P}(\mathrm{x} \le \mathrm{X})} = \frac{\mathrm{C}[\mathrm{Fx}(\mathrm{X}),\ \mathrm{Fy}(\mathrm{Y})]}{\mathrm{Fx}(\mathrm{X})} \quad (4)$$

$$P(y \le Y | x > X) = \frac{Fy(Y) - C[Fx(X), Fy(Y)]}{1 - Fx(X)} \quad (5)$$

Table 2
An overview of the candidate copula functions.

Copula	Expression	Parameter range
Gaussian	$\Phi_\Sigma[\Phi^{-1}(u), \Phi^{-1}(v)]$	/
t	$t_{\Sigma,v}[t_v^{-1}(u), t_v^{-1}(v)]$	/
Clayton	$(u^{-\theta} + v^{-\theta} - 1)^{-1/\theta}$	$\theta \in [-1, +\infty] \backslash \{0\}$
Gumbel	$\exp\{-[(-\ln u)^\theta + (-\ln v)^\theta]^{1/\theta}\}$	$\theta \ge 1$
Frank	$\frac{1}{\theta}\ln[1 + \frac{(e^{-\theta u} - 1)(e^{-\theta v} - 1)}{e^{-\theta} - 1}]$	$\theta \in R \backslash \{0\}$
Joe	$1 - [(1-u)^\theta + (1-v)^\theta + (1-u)^\theta(1-v)^\theta]^{1/\theta}$	$\theta \ge 1$

Table 3
The equations of three distribution functions used in this study.

Distributions	CDF
Normal	$F(x) = \frac{1}{\sqrt{2\pi}}\int_{-\infty}^{x} e^{-t^2/2}dt$
Logistic	$F(x;\ \mu,\ s) = \frac{1}{1 + e^{-(x-\mu)/s}}$
Uniform	$F(x) = \begin{cases} 0 \text{ for } x - \mu < -\sigma\sqrt{3} \\ \frac{1}{2}(\frac{x-\mu}{\sigma\sqrt{3}} + 1) \text{ for } -\sigma\sqrt{3} \le x - \mu < \sigma\sqrt{3} \\ 1 \text{ for } x - \mu \ge \sigma\sqrt{3} \end{cases}$

where P is the probability under specific conditions, C and F are the copula and marginal distributions, x and y represent the value of DI_o and $\Delta Yield$, respectively, X and Y are conditional values of x and y, respectively.

2.5.3. Identifying drought threshold

Note that when the conditional value of $\Delta Yield$ is determined, the yield loss probability increases consistently with more severe drought. Here, we set the probability of yield loss ($\Delta Yield = -0.5$) as 80 %, to obtain the corresponding drought severity. As shown in Eq. (6), the specific derived value of DI_o is the drought threshold (DT) that causes the corresponding yield loss for each shire (Li et al., 2022a).

$$P(\Delta Yield \le -0{\cdot}5 \mid DI_o = DT) = 80\ \% \quad (6)$$

Fig. 2 shows our brief framework. We used the R package of 'SPEI' to calculate the SPI and SPEI (Beguería et al., 2017), 'VineCopula' was used to calculate the joint and conditional probability (Schepsmeier et al., 2015), and 'ggplot2' was used to make the figures (Wickham, 2016).

3. Results

3.1. Correlation between wheat yield variation and drought index

Fig. 3a shows the tau correlation coefficient (τ) between $\Delta Yield$ and 3-, 6-month SPI/SPEI across 66 shires. The average τ value of 3-month SPI had a largest value in September (0.26) while that of 6-month scale SPI was highest in October (0.30) (Fig. 3a). We found similar results for SPEI. Also, we found that regardless of the time scale, the correlation between SPEI and $\Delta Yield$ was slightly higher than SPI in most months. We selected SPEI-6 in October as the optimal drought index (hereinafter referred to as DI_o) capturing wheat yield variation in the study area. Moreover, we found that SPEI-6 in October was significantly correlated with detrended yield calculated by other three methods (Fig. S1-S3). The spatial distribution of the correlation between DI_o and $\Delta Yield$ within the wheat belt is shown in Fig. 3b, with p-values less than 0.05 for 62 shires. We did not consider four shires due to non-significant relation between drought index and yield variation. Moreover, the τ values were higher in the central and western regions than in other parts of the belt.

3.2. Marginal distribution and Copula selection

Table 4 shows the AIC values of the three distribution functions fitted for each shire. The bold number was the minimum AIC among the three distribution functions, with the corresponding distribution being the optimal function. The distribution function of $\Delta Yield$ for most shires was Logistic, and only a few shires were suitable for the Normal distribution.

Once the optimal distribution function of $\Delta Yield$ was determined, we selected the optimal joint distribution function of $\Delta Yield$ and DI_o for each shire from the six alternative copula functions. Fig. 4a depicts the spatial distribution of the optimal copula function in the wheat belt. We found that Clayton was suitable for most shires, with a few shires being suitable for other copula functions of Frank, Gaussian, and t function.

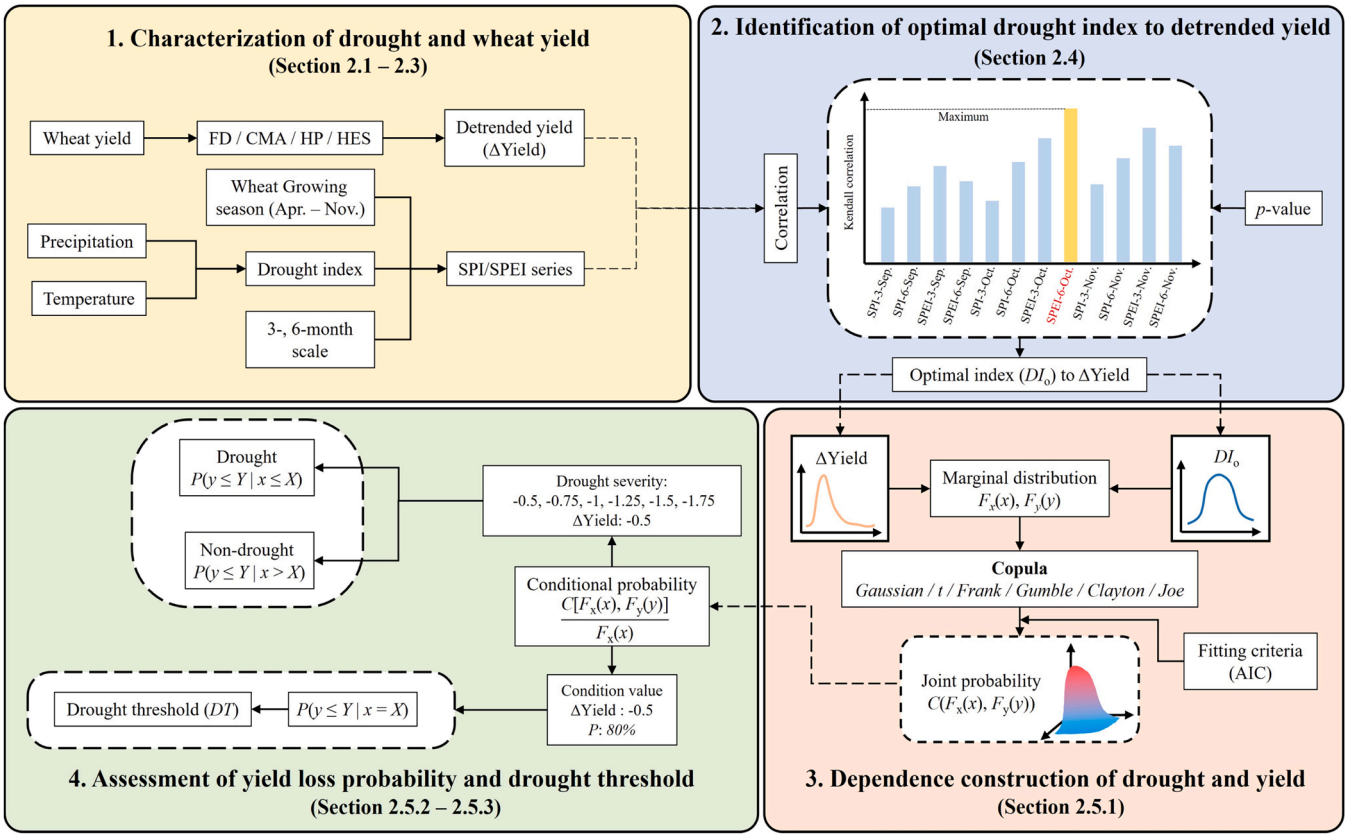

Fig. 2. Schematic diagram of probability evaluation framework of wheat yield loss under different drought severities based on optimal copula functions.

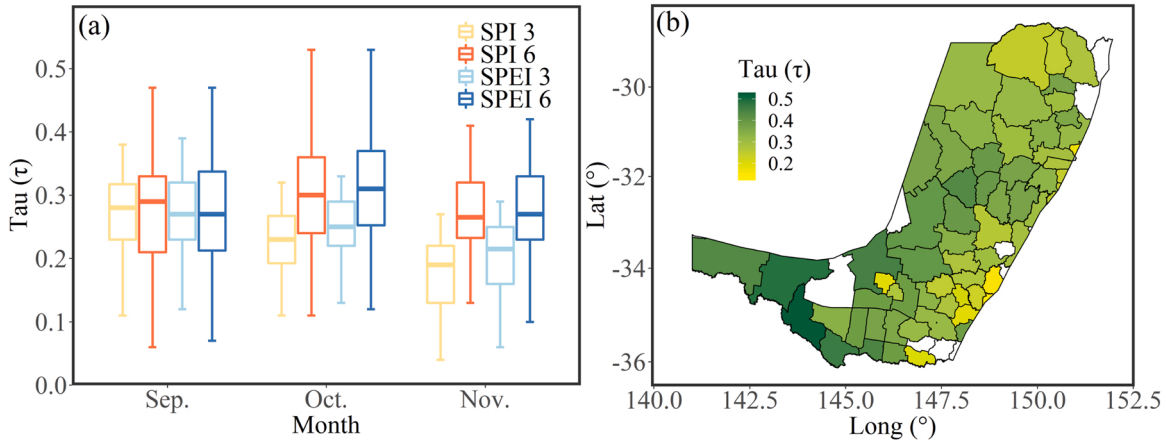

Fig. 3. The tau correlation coefficients (τ) between $\Delta Yield$ and SPI/SPEI calculated in wheat growing season across 66 shires (a), and spatial distribution of τ ($p < 0.05$) between the optimal drought index (SPEI-6 in Oct.) and $\Delta Yield$ for 62 shires (b). Non-significant ($p > 0.05$) shires are shown as blank.

Additionally, similar results were illustrated for other detrended methods (Fig. S4-S6). Note that none of our shires were suitable for Joe and Gumbel copula functions (see Table 2). The spatial distribution of AIC values corresponding to the optimal copula function for each shire showed that the central and southern regions had a slightly lower AIC compared to the other regions (Fig. 4b).

3.3. The probability of yield loss under different drought conditions

We exemplified the conditional probability density values of $\Delta Yield$ at given DI_o values (red shadow) to compare with their pair-wise observed values (black dots) for selected six shires (Fig. 5). The probability density values were normalized into an interval of [0,1] to eliminate the differences in numerical scales of these shires. Most of observed values were located in the red shadow, indicating that the simulated values based on copula function were able to describe the relationship of $\Delta Yield$ and DI_o.

Fig. 6 shows the conditional probability of yield loss under drought ($DI_o \le -0.5$) and non-drought ($DI_o > -0.5$) conditions at six selected representative shires. The yellow percentage in the figure represents the non-exceedance conditional probability of yield loss ($\Delta Yield \le -0.5$) under the drought condition, while the green percent represents the probability under the non-drought condition. The conditional probability of yield loss under the drought condition was much greater than

Table 4
AIC values of three marginal distributions for detrended yield at 62 shires.

Shire	Distribution			Shire	Distribution		
	Normal	Logistic	Uniform		Normal	Logistic	Uniform
Balranald	73.88	**72.85**	90.27	Lockhart	153.87	**144.21**	229.72
Barraba	193.51	**191.67**	242.74	Manilla	192.52	**188.93**	248.38
Berrigan	**122.04**	124.36	139.92	Merriwa	188.03	**182.9**	247.07
Bingara	175.96	**173.37**	233.35	Moree Plains	187.71	**186.55**	230.09
Bland	158.42	**152.96**	210.61	Mudgee	191.76	**183.38**	246.08
Bogan	**165.67**	166.99	198.98	Murray	144.9	**143.31**	191.66
Boorowa	192.68	**187.15**	261.79	Murrumbidgee	**128.1**	130.75	141.22
Cabonne	200.04	**192.83**	263.57	Murrurundi	203.74	**198.26**	263.28
Carrathool	144.89	**138.02**	216.71	Muswellbrook	185.26	**173.33**	285.84
Conargo	**121.57**	123.41	151.86	Narrabri	**178.63**	180.15	208.52
Coolah	189.78	**185.46**	238.98	Narrandera	157.22	**147.36**	240.7
Coolamon	174.12	**167.25**	243.42	Narromine	190.99	**190.03**	217.11
Coonabarabbran	177.76	**173.5**	231.91	Nundle	174.15	**168.42**	236.54
Coonamble	186.7	**183.02**	246.74	Parkes	**180.96**	181.15	219.48
Cootamundra	202.72	**195.41**	262.39	Parry	186.71	**185.94**	232.63
Corowa	146.27	**140.99**	205.12	Quirindi	195.7	**193.51**	232.99
Cowra	189.36	**183.12**	242.74	Rylstone	177.96	**173.29**	228.24
Dubbo	175.58	**172.15**	227.13	Scone	206.63	**181.39**	324.04
Evans	199.87	**182.93**	279.3	Temora	173.63	**166.44**	239.67
Forbes	181.73	**178.99**	230.82	Urana	145.68	**143.16**	186.91
Gilgandra	178.07	**176.5**	226.38	Wagga Wagga	153.49	**144.32**	228.98
Griffith	**51.61**	52.44	74.43	Wakool	142.36	**140.96**	188.35
Gundagai	208.18	**192.5**	297.67	Walgett	**188.66**	192.65	207.25
Gunnedah	190.48	**190.09**	230.09	Warren	**195.41**	197.79	234.42
Harden	185.59	**177.21**	239.33	Weddin	195.46	**190.55**	249.68
Hume	153.98	**143.73**	237.94	Wellington	193.65	**190.91**	241.39
Inverell	170.31	**167.47**	221.04	Wentworth	104.4	**100.43**	124.15
Jerilderie	**122.21**	125.98	130.92	Windouran	166.56	**159.88**	250
Junee	186.35	**178.43**	253.82	Yallaroi	169.87	**166.02**	226.75
Lachlan	157.8	**157.51**	211.44	Yass	179.05	**160.49**	290.38
Leeton	80.32	**74.77**	150.63	Young	193.62	**185.39**	263.87

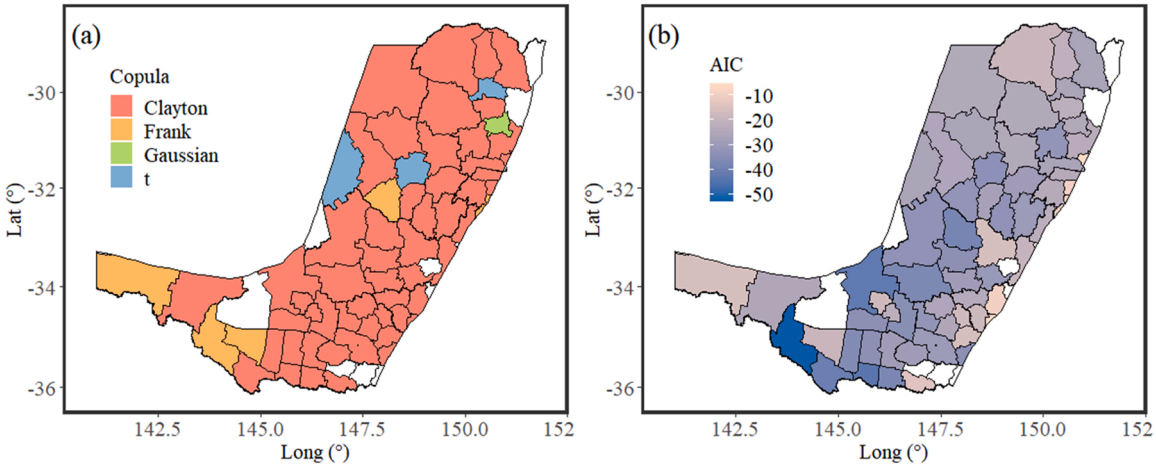

Fig. 4. Optimal copula function between $\Delta Yield$ and DI_o (a) and the corresponding AIC values (b) in the NSW wheat belt.

that under the non-drought condition, indicating that drought was more likely to cause yield loss. The probability value for ND in region 3 was smallest, with only 35 %, if only considering the probability of yield loss that occurred under drought condition. The drought conditional probability at NM in region 2 was highest with 53.3 %. Under the non-drought condition, the probability of yield loss was 13.7 % and 13 % at ND and HB, respectively, which was higher than other shires. This might be due to the higher rainfall in these two shires, thus the probability of yield loss caused by non-drought factors like (such as water-logging) was higher than that in other shires. It is notable that yield loss probability under non-drought condition was only 4.4 % for WK as it was the driest in six selected shires.

Fig. 7 shows the spatial distribution of yield loss probability across the wheat belt under different drought severities. In general, the loss probability of yield increased as the increase of drought severity. For example, the average probability of yield loss was 50.1 % when DI_o was less than −0.5, but the probability of yield loss increased to 88.6 % under severer drought conditions ($DI_o \leq -1.5$). We also calculated the yield loss probability due to different drought severities for each region (Fig. 8). Generally, under drought condition, the yield loss probabilities in all three regions tended to increase as drought severity increased. The yield loss probability was lowest in region 3, indicating that it was less affected by drought compared to other two regions. The yield loss probability was close (higher than 75 %) for region 1 and region 2 when moderate and severe drought occurred. The results based on other three detrended methods of CMA, HP, and HES also showed that yield loss

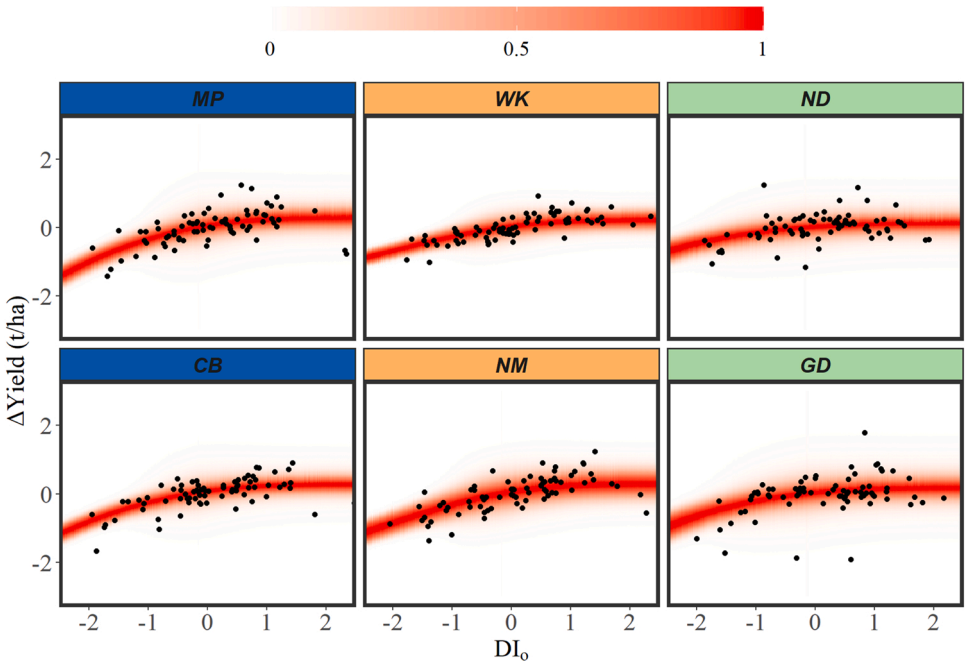

Fig. 5. Simulated (red shadows) and observed (black dots) pairwise values of Δ*Yield* and DI_o for Coonabarabbran (CB), Moree Plains (MP), Wakool (WK), Narromine (NM), Nundle (ND), and Gundagai (GD). The colour represents the normalized probability density values of Δ*Yield* at given DI_o values calculated by corresponding probability density functions (PDF).

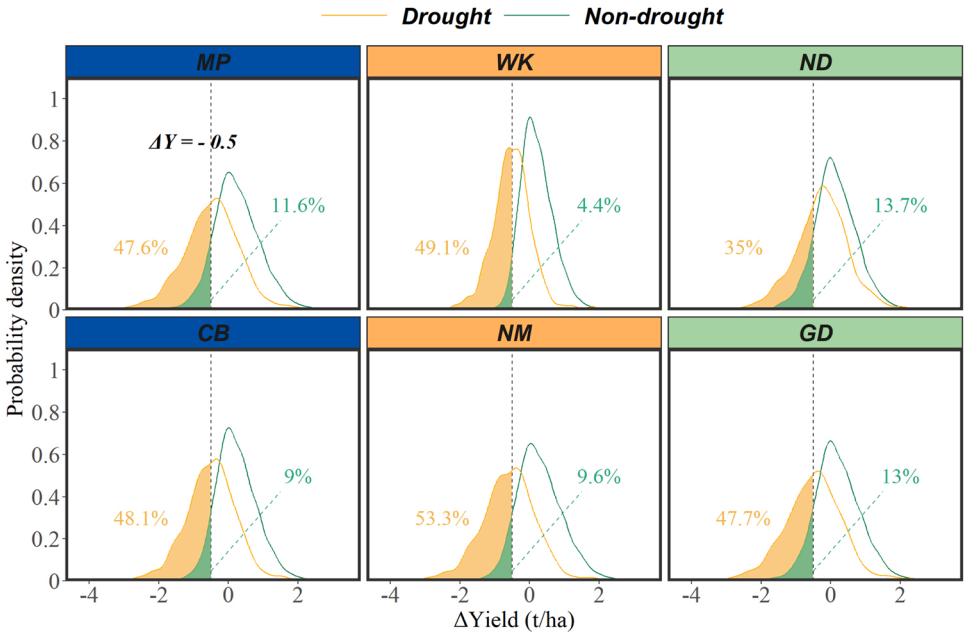

Fig. 6. Yield loss probability density curves under drought ($DI_o < -0.5$) and non-drought ($DI_o > -0.5$) conditions at Coonabarabbran (CB), Moree Plains (MP), Wakool (WK), Narromine (NM), Nundle (ND), and Gundagai (GD). The black vertical dashed line is the conditional value of yield loss (Δ*Yield* = −0.5). The yellow and green lines are probability density line under drought and non-drought conditions, respectively. The yellow and green shadow areas represent the probability of yield loss under drought and non-drought conditions, respectively.

probability in region 3 was lowest compared to other two regions (Fig. S16 – S18).

The drought threshold for each region and shire was shown in Fig. 9. We found that averaged drought threshold value increased from region 3 (−2.18) to region 1 (−1.62) (Fig. 9a). Also, *DT* in the shires of western NSW wheat belt had higher values than those shires in eastern Australia (Fig. 9b). These results indicated that the wheat yield in northwest region was more sensitive to drought than that in eastern high-rainfall region. Other detrended methods illustrated similar distribution of *DT* except the CMA method. Specifically, CMA method showed that the averaged drought threshold of region 2 was slightly higher than region 1 (Fig. S19a).

4. Discussion

We firstly investigated the relationship between the detrended yield and drought index. Then we established the joint probability model to estimate the yield loss risk under various drought severities based on the conditional probability theory. Moreover, we derived the drought thresholds triggering same level of yield loss for each shire. As far as we know, our study represents the first instance of utilizing a copula-based method to conduct a probabilistic assessment of the impact of drought events on wheat yields in Australia at a local scale (shire level). Additionally, our study also quantifies the specific drought thresholds that trigger yield loss. We expect our method could be used in other major

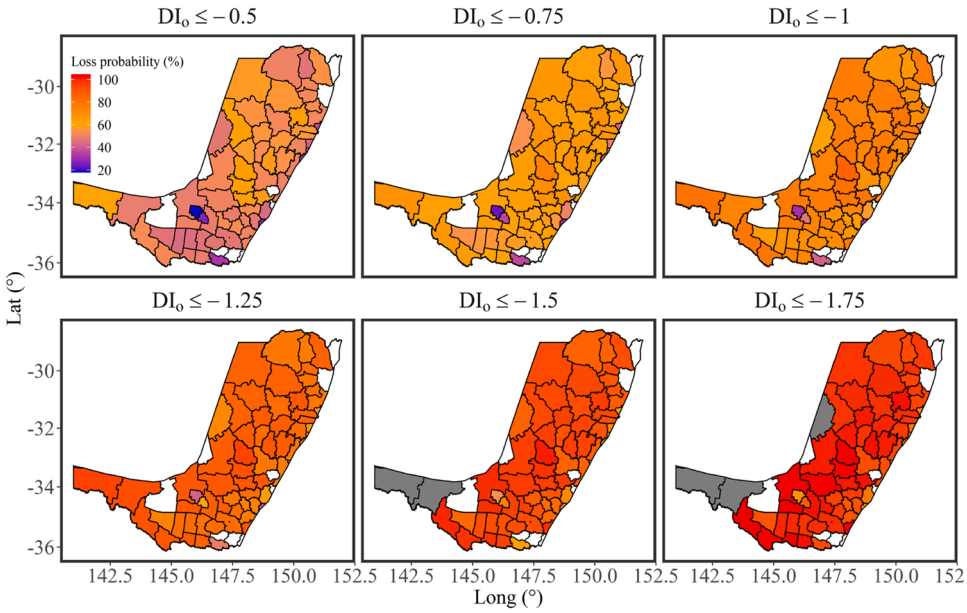

Fig. 7. Spatial distribution of yield loss probability under different drought severities. Shires in grey indicating that the conditional values of DI_o are too extreme to estimate the yield loss probability with copula function.

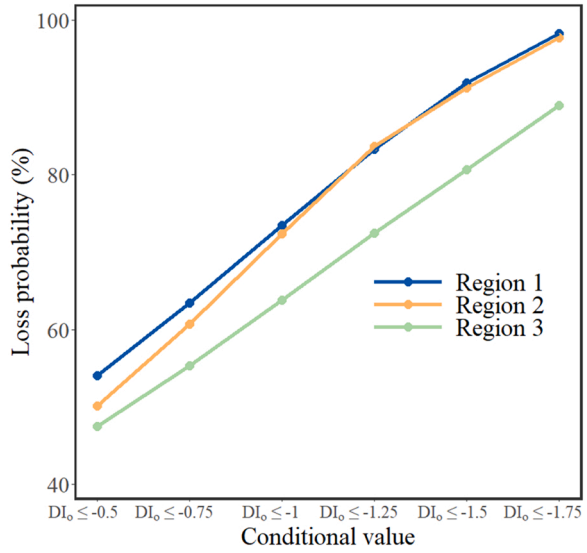

Fig. 8. Regional average of yield loss probability under different drought severities.

rainfed cropping regions around the world where crops often suffer from drought stress.

Previous studies have emphasized the characteristics between crop yield and drought indices with different time scales (Hunt et al., 2014; Zipper et al., 2016). Our study provided further evidence. For example, we found that, among all four detrended methods, the 6-month SPEI in October exhibited the strongest correlation with the variability of detrended wheat yield across the wheat belt region in NSW. These findings are consistent with results from previous studies. For example, Peña-Gallardo et al. (2019) analysed the response of several crop yields to different time scales of drought indices in the U.S., and they found that a high correlation occurs between winter wheat yield and 6-month SPEI. Usually, wheat is sowed in May and harvested in November in the Australian wheat belt, and thus, the 6-month scale covers the most growth periods of wheat. Therefore, the climatic change during this period could better explain the variability of wheat yield than 3-month index. However, the correlation between SPEI and detrended yield is only slightly better than that of SPI (Fig. 3), indicating that the sensitivity of drought index to capture yield variation is not significantly improved by taking PET into account. This is likely due to the equation used to estimate PET only considering temperature. However, the PET can be affected by many other climatic factors, such as wind speed and humidity (Shi et al., 2022; Xiang et al., 2020).

We found that the Clayton was the optimal copula function for most of our shires among four detrended methods (Fig. 4, S4-S6), revealing that a strong lower tail dependence between the time series of detrended yield and SPEI existed in most shires (Du et al., 2018; She and Xia, 2018). The comparison of simulated conditional probability of detrended yield and drought index with corresponding pair-wise observed value, illustrated that most of the observed samples fall within the probability density range estimated by the Clayton copula function. Additionally, a small number of samples deviated from this range, possibly due to anomalous weather in the corresponding year (Potgieter et al., 2013). The yield loss probabilities under drought condition were much higher than that under non-drought condition (Fig. 6). We suspect that other factors such as excessive water supply had limited effects on wheat yield under non-drought condition (Cossani and Sadras, 2018; Sadras et al., 2016).

The yield loss probability under different drought severities illustrates a tendency that as the severity level of drought increases, the probability of wheat yield loss gradually increases (Fig. 7), which is consistent with previous studies (Li et al., 2022a; Liu et al., 2022). The severity of drought represents the adequacy of the water supply required for wheat growth. More severe droughts have greater water deficit. During drought conditions, the limited availability of water significantly constrains the growth of wheat and has a pronounced impact on its yield (Asseng et al., 2004; Song et al., 2019), thus increasing the probability of yield loss. Under severe drought conditions, the water deficit becomes the dominant factor affecting the growth and leading to the increase of the yield loss probability. As the severity tends to extreme levels, the yield loss probability approaches to 100 % for several shires if no measures are taken to interfere with this process. The results of conditional probability showed that the copula function was capable of capturing the probability variations of yield loss at the shire scale.

In addition, yield loss probability varied regionally (Fig. 8). The loss probability in region 1 was highest, followed by region 2 and region 3.

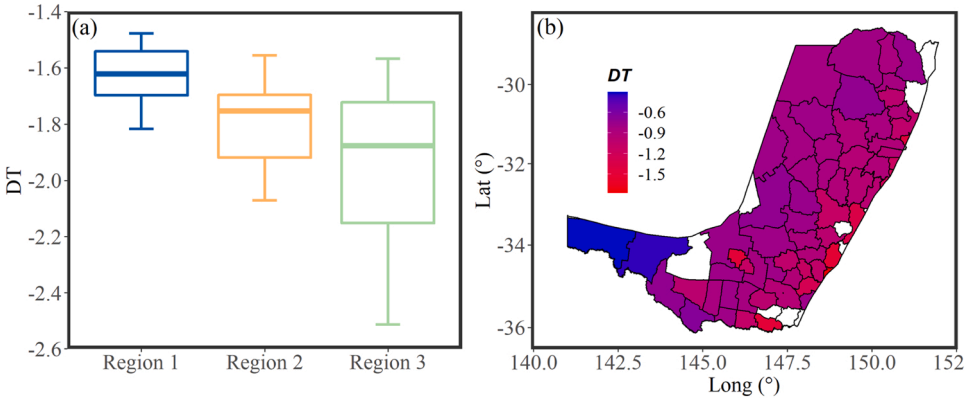

Fig. 9. Drought threshold (*DT*) for each region (a) and shire (b) when the probability of yield loss ($\Delta Yield \leq -0.5$) is 80 % in the NSW wheat belt.

The growing season rainfall decreased from the east to west, and the temperature decrease from the northwest to the southeast in the wheat belt. We anticipate that the region 1 is under the dry and hot climate conditions with more severe water shortage compared to region 3 with a cool and moist climate (Feng and Wang, 2019b). Although the soil in region 1 has a high water holding capacity (Page et al., 2018), the rain mainly falls in the summer. By contrast, the rainfall of region 2 mainly occurs in winter. As a result, the water for wheat growth can be recharged to some extent.

Additionally, we quantified the drought threshold for each region (Fig. 9). Although the results of CMA detrended method depicted a little difference from other methods, the drought threshold of region 1 was highest, followed by region 2 and region 3. The values of drought threshold represent the sensitivity of wheat yield to drought. We speculate that region 1 was the most sensitive to drought, and region 3 had a less sensitivity to drought. Therefore, some targeted actions are required to lower the loss probability of wheat yield in drought sensitive regions, especially as drought severity continues to worsen. For example, drought-tolerant wheat cultivars should be considered to enhance the drought resistance for region 1 and 2 (Wang et al., 2019). The management practices, such as sowing dates, could be adjusted to avoid the impact of drought on critical growth stages of wheat (Chen et al., 2020a; Zeleke and Nendel, 2016; Zhao et al., 2015). Moreover, implementing a crop rotation system featuring well-suited crops and wheat, using the right amount of fertilizer, and employing practical agronomy options such as stubble return, can enhance both the drought resistance and agricultural benefits of this region (Edwards, 2000; Ryan et al., 2008; Sedri et al., 2019). Therefore, our results can help government agencies to identify the hotspots that are vulnerable to drought conditions and enable local growers to employ effective agronomic options to cope with extreme drought.

There are some limitations in our study. Firstly, the research period for wheat yield only covered 1922–2000. The lack of recent wheat yield data for each shire prevents us evaluating the yield loss risk in the latest decades when the occurrence of drought years has increased. Crop model has been widely used to simulate crop yield forced with climate data. It is possible to employ APSIM model to obtain wheat yield in a long-term period (e.g., 1900–2022) for each study shire. Then the simulated yield can be used to quantify the drought impact (Leng and Hall, 2019). Secondly, using SPEI or SPI to characterize the drought condition is partially inadequate since only the precipitation and temperature were considered (Beguería et al., 2014). There are other factors that can affect the wheat growth and yield, such as soil properties (Ding et al., 2020a; Ko et al., 2010). For example, clay soil has a better buffer capacity to cope with drought than sandy soil (Karhu et al., 2011; Olmo et al., 2016). Thus, soil moisture-related drought indices should be used to provide more comprehensive information of agricultural drought impacts on crop production. Furthermore, more correlation methods should be considered to provide robust results for optimal drought index selection (Pan et al., 2019). Lastly, other extreme climate events, such as heat and frost, often accompany drought. Zhao et al. (2022) evaluated the shock trend of wheat yield loss under hot-dry-windy events of USA wheat belt. They found that the compound events can lead to the 4 % of yield reduction. Moreover, global warming is projected to result in the more frequent compound events in the future (Hao and Singh, 2020; Meng et al., 2022), especially for the cropland (Lesk and Anderson, 2021). Therefore, we recommend that future work should pay attention towards understanding the impacts of compound drought and heat events on crop yield in rainfed areas.

5. Conclusion

For the first time, we developed a probabilistic analysis method rather than using a deterministic approach to quantify the yield loss probability under various drought severities at a shire scale in the NSW wheat belt, south-eastern Australia. We also empirically determined the drought threshold for each shire based on the copula functions. We found that the 6-month SPEI could well explain the variability of detrended wheat yield, although taking evapotranspiration into account did not significantly improve the correlation coefficients between drought index and detrended yield. Due to diverse climatic patterns in the wheat belt, our results showed that both yield loss possibility and drought threshold were region-specific. We found that the western study area was more sensitive to drought. Therefore, more effective agronomic options were required to mitigate the risk of yield loss in these drought-prone regions.

A probabilistic investigation of yield variability under drought severity is more valuable than the results of using deterministic method for risk management policy makers and agricultural insurance evaluators. The vulnerable hotspots can be quickly identified, and their dynamic change could be effectively detected based on the climatic variability. We expect that our research framework can be extended to other areas, particularly in the context of more frequent drought events, by integrating compound events such as drought and heat with crop models under future climate scenarios.

Declaration of Competing Interest

The authors declare that they have no known competing financial interests or personal relationships that could have appeared to influence the work reported in this paper.

Data availability

Data will be made available on request.

Acknowledgements

The first author acknowledges the China Scholarship Council (CSC No. 202006300006) for the financial support of his Ph.D. study. Facilities for conducting this study were provided by the New South Wales Department of Primary Industries and University of Technology Sydney. Bernie Dominiak reviewed the manuscript.

Appendix A. Supporting information

Supplementary data associated with this article can be found in the online version at doi:10.1016/j.agwat.2023.108359.

References

Araneda-Cabrera, R.J., Bermúdez, M., Puertas, J., 2021. Benchmarking of drought and climate indices for agricultural drought monitoring in Argentina. Sci. Total Environ. 790 (2021), 1–12.
Asseng, S., et al., 2004. Simulated wheat growth affected by rising temperature, increased water deficit and elevated atmospheric CO_2. Field Crops Res. 85 (2–3), 85–102.
Beguería, S., Vicente-Serrano, S.M., Reig, F., Latorre, B., 2014. Standardized precipitation evapotranspiration index (SPEI) revisited: parameter fitting, evapotranspiration models, tools, datasets and drought monitoring. Int. J. Clim. 34 (10), 3001–3023.
Beguería, S., Vicente-Serrano, S.M., Beguería, M.S.J., 2017. Package 'spei'. Calculation of the Standardised Precipitation-Evapotranspiration Index. CRAN 2017 (1), 1–13.
Bonett, D.G., Wright, T.A., 2000. Sample size requirements for estimating Pearson, Kendall and Spearman correlations. Psychometrika 65 (1), 23–28.
Chang, J., et al., 2019. Reservoir operations to mitigate drought effects with a hedging policy triggered by the drought prevention limiting water level. Water Resour. Res. 55 (2), 904–922.
Chen, C., et al., 2020a. The shifting influence of future water and temperature stress on the optimal flowering period for wheat in Western Australia. Sci. Total Environ. 737 (2020), 1–12.
Chen, X., et al., 2020b. Impacts of multi-timescale SPEI and SMDI variations on winter wheat yields. Agric. Syst. 185 (2020), 1–14.
Cheng, J., Yin, S., 2021. Analysis of drought characteristics and its effects on crop yield in Xinjiang in recent 60 years. Sustainability 13 (24), 13833.
Chiang, F., Mazdiyasni, O., AghaKouchak, A., 2021. Evidence of anthropogenic impacts on global drought frequency, duration, and intensity. Nat. Commun. 12 (1), 1–10.
Christian, J.I., et al., 2021. Global distribution, trends, and drivers of flash drought occurrence. Nat. Commun. 12 (1), 1–11.
Cossani, C.M., Sadras, V.O., 2018. Water–nitrogen colimitation in grain crops. Adv. Agron. 150 (2018), 231–274.
Croux, C., Dehon, C., 2010. Influence functions of the Spearman and Kendall correlation measures. Stat. Methods Appl. 19 (4), 497–515.
Daryanto, S., Wang, L., Jacinthe, P.-A., 2016. Global synthesis of drought effects on maize and wheat production. PloS One 11 (5), 1–15.
Deb, P., Moradkhani, H., Han, X., Abbaszadeh, P., Xu, L., 2022. Assessing irrigation mitigating drought impacts on crop yields with an integrated modeling framework. J. Hydrol. 609 (2022), 1–19.
Ding, J., Hu, W., Wu, J., Yang, Y., Feng, H., 2020a. Simulating the effects of conventional versus conservation tillage on soil water, nitrogen dynamics, and yield of winter wheat with RZWQM2. Agric. Water Manag. 230 (2020), 1–8.
Ding, Y., Xu, J., Wang, X., Peng, X., Cai, H., 2020b. Spatial and temporal effects of drought on Chinese vegetation under different coverage levels. Sci. Total Environ. 716 (2020), 1–12.
Du, X., Hennessy, D.A., Feng, H., Arora, G., 2018. Land resilience and tail dependence among crop yield distributions. Am. J. Agric. Econ. 100 (3), 809–828.
Edwards, J., 2000. Western farming systems project. Grains Research & Development Corporation.
Feng, P., et al., 2018. Impacts of rainfall extremes on wheat yield in semi-arid cropping systems in eastern Australia. Clim. Change 147 (3), 555–569.
Feng, P., et al., 2019a. Projected changes in drought across the wheat belt of southeastern Australia using a downscaled climate ensemble. Int. J. Clim. 39 (2), 1041–1053.
Feng, P., Wang, B., Li Liu, D., Waters, C., Yu, Q., 2019b. Incorporating machine learning with biophysical model can improve the evaluation of climate extremes impacts on wheat yield in south-eastern Australia. Agr. For. Meteorol. 275 (2019), 100–113.
Feng, S., Hao, Z., 2020. Quantifying likelihoods of extreme occurrences causing maize yield reduction at the global scale. Sci. Total Environ. 704 (2020), 1–8.
Fitzsimmons, R., 2001. Winter Cereal Production Statistics, NSW 1922–1999: Wheat, Oats, Barley: Area Production and Yield: NSW by Local Government Areas, Individual Years plus 5 and 10 Year Averages. Australian Institute of Agricultural Science and Technology, 6th edn(Wahroonga).
Godfrey, S.S., Ip, R.H., Nordblom, T.L., 2022. Risk Analysis of Australia's Victorian Dairy Farms Using Multivariate Copulae. J. Agric. Appl. Econ. 54 (1), 72–92.
Grundy, M.J., et al., 2016. Scenarios for Australian agricultural production and land use to 2050. Agric. Syst. 142 (2016), 70–83.
Haile, G.G., et al., 2020. Long-term spatiotemporal variation of drought patterns over the Greater Horn of Africa. Sci. Total Environ. 704 (1), 1–13.
Hao, Z., Singh, V.P., 2020. Compound events under global warming: a dependence perspective. J. Hydrol. Eng. 25 (9), 1–8.
Harvey, A., Trimbur, T., 2008. Trend estimation and the Hodrick-Prescott filter. J. Jpn. Stat. Soc. 38 (1), 41–49.
He, P., et al., 2022. Compound drought constrains gross primary productivity in Chinese grasslands. Environ. Res. Lett. 17 (10), 1–12.
Holt, C.C., 2004. Forecasting seasonals and trends by exponentially weighted moving averages. Int. J. Forecast. 20 (1), 5–10.
Hoover, D.L., et al., 2022. Compound hydroclimatic extremes in a semi-arid grassland: Drought, deluge, and the carbon cycle. Glob. Change Biol. 28 (8), 2611–2621.
Hunt, E.D., et al., 2014. Monitoring the effects of rapid onset of drought on non-irrigated maize with agronomic data and climate-based drought indices. Agr. For. Meteorol. 191 (2014), 1–11.
Jeffrey, S.J., Carter, J.O., Moodie, K.B., Beswick, A.R., 2001. Using spatial interpolation to construct a comprehensive archive of Australian climate data. Environ. Modell. Softw. 16 (4), 309–330.
Kamali, B., et al., 2022. Probabilistic modeling of crop-yield loss risk under drought: a spatial showcase for sub-Saharan Africa. Environ. Res. Lett. 17 (2), 1–13.
Kamali, B., Abbaspour, K., Lehmann, A., Wehrli, B., Yang, H., 2015. Identification of spatiotemporal patterns of biophysical droughts in semi-arid region–a case study of the Karkheh river basin in Iran. Hydrol. Earth Syst. Sci. Discuss. 12 (6), 5187–5217.
Karhu, K., Mattila, T., Bergström, I., Regina, K., 2011. Biochar addition to agricultural soil increased CH4 uptake and water holding capacity–Results from a short-term pilot field study. Agric., Ecosyst. Environ. 140 (1–2), 309–313.
Ko, J., et al., 2010. Simulation of free air CO_2 enriched wheat growth and interactions with water, nitrogen, and temperature. Agr. For. Meteorol. 150 (10), 1331–1346.
Labudová, L., Labuda, M., Takáč, J., 2017. Comparison of SPI and SPEI applicability for drought impact assessment on crop production in the Danubian Lowland and the East Slovakian Lowland. Theor. Appl. Clim. 128 (1), 491–506.
Leng, G., 2021. Maize yield loss risk under droughts in observations and crop models in the United States. Environ. Res. Lett. 16 (2), 1–10.
Leng, G., Hall, J., 2019. Crop yield sensitivity of global major agricultural countries to droughts and the projected changes in the future. Sci. Total Environ. 654 (2019), 811–821.
Lesk, C., Anderson, W., 2021. Decadal variability modulates trends in concurrent heat and drought over global croplands. Environ. Res. Lett. 16 (5), 1–14.
Li, H., Li, Y., Huang, G., Sun, J., 2021. Probabilistic assessment of crop yield loss to drought time-scales in Xinjiang. China Int. J. Clim. 41 (8), 4077–4094.
Li, P., et al., 2022a. Various maize yield losses and their dynamics triggered by drought thresholds based on Copula-Bayesian conditional probabilities. Agric. Water Manag. 261 (2022), 1–12.
Li, Q., Chen, L., Xu, Y., 2022b. Drought risk and water resources assessment in the Beijing-Tianjin-Hebei region. China Sci. Total Environ. 832 (2022), 1–15.
Li, S., et al., 2022c. Assessing climate vulnerability of historical wheat yield in south-eastern Australia's wheat belt. Agric. Syst. 196 (2022), 103340.
Li, X., 2013. Comparison and analysis between holt exponential smoothing and brown exponential smoothing used for freight turnover forecasts, 2013 Third International Conference on Intelligent System Design and Engineering Applications. IEEE, pp. 453–456.
Liu, D., Anwar, M.R., O'Leary, G., Conyers, M.K., 2014. Managing wheat stubble as an effective approach to sequester soil carbon in a semi-arid environment: Spatial modelling. Geoderma 214 (2014), 50–61.
Liu, S., et al., 2022. Probability of maize yield failure increases with drought occurrence but partially depends on local conditions in China. Eur. J. Agron. 139 (2022), 1–9.
Loukas, A., Vasiliades, L., Tzabiras, J., 2008. Climate change effects on drought severity. Adv. Geosci. 17 (2008), 23–29.
Lu, J., Carbone, G.J., Gao, P., 2017. Detrending crop yield data for spatial visualization of drought impacts in the United States, 1895–2014. Agr. For. Meteorol. 237 (2017), 196–208.
Madadgar, S., AghaKouchak, A., Farahmand, A., Davis, S.J., 2017. Probabilistic estimates of drought impacts on agricultural production. Geophys. Res. Lett. 44 (15), 7799–7807.
McKee, T.B., Doesken, N.J. and Kleist, J., 1993. The relationship of drought frequency and duration to time scales, Proceedings of the 8th Conference on Applied Climatology. California, pp. 179–183.
Meng, Y., Hao, Z., Feng, S., Zhang, X., Hao, F., 2022. Increase in compound dry-warm and wet-warm events under global warming in CMIP6 models. Glob. Planet. Change 210 (2022), 103773.
Meza, I., et al., 2021. Drought risk for agricultural systems in South Africa: Drivers, spatial patterns, and implications for drought risk management. Sci. Total Environ. 799 (2021), 1–14.
Mokhtar, A., et al., 2022. Assessment of the effects of spatiotemporal characteristics of drought on crop yields in southwest China. Int. J. Clim. 42 (5), 3056–3075.
Nelsen, R.B., 2007. An introduction to copulas. Springer Science & Business Media.
Olmo, M., Lozano, A.M., Barrón, V., Villar, R., 2016. Spatial heterogeneity of soil biochar content affects soil quality and wheat growth and yield. Sci. Total Environ. 562 (2016), 690–700.
Page, K., et al., 2018. Management of the major chemical soil constraints affecting yields in the grain growing region of Queensland and New South Wales. Aust. Rev. Soil Res 56 (8), 765–779.
Pan, J.-J., Mahmoudi, M.R., Baleanu, D., Maleki, M., 2019. On comparing and classifying several independent linear and non-linear regression models with symmetric errors. Symmetry 11 (6), 820–825.
Patton, A., 2012. A review of copula models for economic time series. J. Multiv. Anal. 110 (2012), 4–18.

Peña-Gallardo, M., et al., 2019. Response of crop yield to different time-scales of drought in the United States: Spatio-temporal patterns and climatic and environmental drivers. Agr. For. Meteorol. 264 (2019), 40–55.
Poonia, V., Jha, S., Goyal, M.K., 2021. Copula based analysis of meteorological, hydrological and agricultural drought characteristics across Indian river basins. Int. J. Clim. 41 (9), 4637–4652.
Potgieter, A., et al., 2013. Spatial impact of projected changes in rainfall and temperature on wheat yields in Australia. Clim. Change 117 (1), 163–179.
Prodhan, F.A., et al., 2022. Projection of future drought and its impact on simulated crop yield over South Asia using ensemble machine learning approach. Sci. Total Environ. 807 (2022), 1–15.
Ray, D.K., Gerber, J.S., MacDonald, G.K., West, P.C., 2015. Climate variation explains a third of global crop yield variability. Nat. Commun. 6 (1), 1–9.
Ribeiro, A.F., Russo, A., Gouveia, C.M., Páscoa, P., 2019a. Copula-based agricultural drought risk of rainfed cropping systems. Agric. Water Manag. 223 (2019), 1–11.
Ribeiro, A.F., Russo, A., Gouveia, C.M., Páscoa, P., Pires, C.A., 2019b. Probabilistic modelling of the dependence between rainfed crops and drought hazard. Nat. Hazards Earth Syst. Sci. 19 (12), 2795–2809.
Ryan, J., Pala, M., Masri, S., Singh, M., Harris, H., 2008. Rainfed wheat-based rotations under Mediterranean conditions: Crop sequences, nitrogen fertilization, and stubble grazing in relation to grain and straw quality. Eur. J. Agron. 28 (2), 112–118.
Sadras, V., et al., 2016. Interactions between water and nitrogen in Australian cropping systems: physiological, agronomic, economic, breeding and modelling perspectives. Crop Pasture Sci. 67 (10), 1019–1053.
Sakamoto, Y., Ishiguro, M., Kitagawa, G., 1986. Akaike information criterion statistics. Dordrecht. In: The Netherlands: D. Reidel, 81, p. 26853.
Schepsmeier, U., et al., 2015. Package 'vinecopula'. R. Package Version 2 (5), 1–148.
Sedri, M.H., Amini, A., Golchin, A., 2019. Evaluation of nitrogen effects on yield and drought tolerance of rainfed wheat using drought stress indices. J. Crop Sci. Biotechnol. 22 (2019), 235–242.
She, D., Xia, J., 2018. Copulas-based drought characteristics analysis and risk assessment across the Loess Plateau of China. Water Resour. Manag. 32 (2), 547–564.
Shi, L., et al., 2022. Assessing future runoff changes with different potential evapotranspiration inputs based on multi-model ensemble of CMIP5 projections. J. Hydrol. 612 (2022), 1–13.
Sklar, A., 1973. Random variables, joint distribution functions, and copulas. Kybernetika 9 (6), 449–460.
Soľáková, T., De Michele, C., Vezzoli, R., 2014. Comparison between parametric and nonparametric approaches for the calculation of two drought indices: SPI and SSI. J. Hydrol. Eng. 19 (9), 1–11.
Song, L., Jin, J., He, J., 2019. Effects of severe water stress on maize growth processes in the field. Sustainability 11 (18), 1–10.
Steve, H.-D., Neal, H., Andrew, C., Matthew, M., Tom, J., 2018. Analysis of 2018 drought. ABARES Insights 2018 (2), 1–7.
Sun, P., Liu, R., Yao, R., Shen, H., Bian, Y., 2023. Responses of agricultural drought to meteorological drought under different climatic zones and vegetation types. J. Hydrol. 619 (2023), 1–12.
Szalai, S., Szinell, C., 2000. Comparison of two drought indices for drought monitoring in Hungary—a case study. Drought and drought mitigation in Europe. Springer, pp. 161–166.
Tao, F., Yokozawa, M., Liu, J., Zhang, Z., 2008. Climate–crop yield relationships at provincial scales in China and the impacts of recent climate trends. Clim. Res 38 (1), 83–94.
Temizhan, E., Mirtagioglu, H., Mendes, M., 2022. Which Correlation Coefficient Should Be Used for Investigating Relations between Quantitative Variables? Am. Acad. Sci. Res. J. Eng., Tech., Sci. 85 (1), 265–277.
Thornthwaite, C.W., 1948. An Approach toward a Rational Classification of Climate. Geogr. Rev. 38 (1), 55–94.
Vicente-Serrano, S.M., Beguería, S., López moreno, J.I., 2010. A multiscalar drought index sensitive to global warming: the standardized precipitation evapotranspiration index. J. Clim. 23 (7), 1696–1718.
Waha, K., et al., 2022. Past and future rainfall changes in the Australian midlatitudes and implications for agriculture. Clim. Change 170 (3–4), 29.
Wambua, R.M., 2019. Spatio-temporal characterization of Agricultural Drought using Soil Moisture Deficit Index (SMDI) in the Upper Tana River basin, Kenya. Int. J. Eng. Res. Adv. Tech. 5 (2), 93–106.
Wang, B., et al., 2015a. Effects of climate trends and variability on wheat yield variability in eastern Australia. Clim. Res. 64 (2), 173–186.
Wang, B., et al., 2019. Designing wheat ideotypes to cope with future changing climate in South-Eastern Australia. Agric. Syst. 170 (2019), 9–18.
Wang, W., Zhu, Y., Xu, R., Liu, J., 2015b. Drought severity change in China during 1961–2012 indicated by SPI and SPEI. Nat. Hazards 75 (3), 2437–2451.
Wickham, H., 2016. Data analysis. Springer.
Won, J., Choi, J., Lee, O., Kim, S., 2020. Copula-based Joint Drought Index using SPI and EDDI and its application to climate change. Sci. Total Environ. 744 (2020), 140701.
Xiang, K., Li, Y., Horton, R., Feng, H., 2020. Similarity and difference of potential evapotranspiration and reference crop evapotranspiration -a review. Agric. Water Manag. 232 (2020), 1–16.
Yang, Y., et al., 2016. Contrasting responses of water use efficiency to drought across global terrestrial ecosystems. Sci. Rep. 6 (1), 1–8.
Yin, J., et al., 2022. Global increases in lethal compound heat stress: Hydrological drought hazards under climate change. Geophys. Res. Lett. 49 (18), 1–12.
Zarei, A.R., Shabani, A., Mahmoudi, M.R., 2019. Comparison of the climate indices based on the relationship between yield loss of rain-fed winter wheat and changes of climate indices using GEE model. Sci. Total Environ. 661 (2019), 711–722.
Zargar, A., Sadiq, R., Naser, B., Khan, F.I., 2011. A review of drought indices. Environ. Rev. 19 (2011), 333–349.
Zeleke, K., Nendel, C., 2016. Analysis of options for increasing wheat (Triticum aestivum L.) yield in south-eastern Australia: The role of irrigation, cultivar choice and time of sowing. Agric. Water Manag. 166 (2016), 139–148.
Zhang, F., et al., 2019. Dynamic drought risk assessment for maize based on crop simulation model and multi-source drought indices. J. Clean. Prod. 233 (2019), 100–114.
Zhang, T., Zhu, J., Wassmann, R., 2010. Responses of rice yields to recent climate change in China: an empirical assessment based on long-term observations at different spatial scales (1981–2005). Agr. For. Meteorol. 150 (7–8), 1128–1137.
Zhang, X., Jiang, H., 2019. Application of Copula function in financial risk analysis. Comput. Elect. Eng. 77 (2019), 376–388.
Zhao, H., et al., 2022. US winter wheat yield loss attributed to compound hot-dry-windy events. Nat. Commun. 13 (1), 1–9.
Zhao, J., Yang, X., Dai, S., Lv, S., Wang, J., 2015. Increased utilization of lengthening growing season and warming temperatures by adjusting sowing dates and cultivar selection for spring maize in Northeast China. Eur. J. Agron. 67 (2015), 12–19.
Zipper, S.C., Qiu, J., Kucharik, C.J., 2016. Drought effects on US maize and soybean production: spatiotemporal patterns and historical changes. Environ. Res. Lett. 11 (9), 1–12.